Electrochimica Acta 58 (2011) 532–540

Contents lists available at SciVerse ScienceDirect

Electrochimica Acta

journal homepage: www.elsevier.com/locate/electacta

New insight into indium electrochemistry in a Tf_2N-based room-temperature ionic liquid

Youssouf Traore[a,1], Sophie Legeai[b,*,2,3], Sébastien Diliberto[b,3], Guilhem Arrachart[c,4], Stéphane Pellet-Rostaing[c,5], Micheline Draye[a,**,6]

[a] Laboratoire de Chimie Moléculaire et Environnement, Université de Savoie, Campus scientifique, 73376 Le Bourget-du-Lac Cedex, France
[b] Institut Jean Lamour, UMR 7198, Groupe Chimie et Electrochimie des Matériaux, Université Paul Verlaine – Metz, 1 boulevard Arago, 57078 Metz Cedex 3, France
[c] Institut de Chimie Séparative de Marcoule, CNRS/CEA/ENSCM, UMR 5257, Laboratoire Tri ionique par les Systèmes Moléculaires auto-assemblés, Bât. 406, route de Marcoule, 30207 Bagnols-sur-Cèze, France

ARTICLE INFO

Article history:
Received 25 July 2011
Received in revised form
21 September 2011
Accepted 30 September 2011
Available online 20 October 2011

Keywords:
Piperidinium
Ionic liquid
Indium
Electrodeposition

ABSTRACT

The electrodeposition of indium is reported in a new weakly hygroscopic piperidinium-based ionic liquid (1-butyl-1-ethyl-piperidinium bis(trifluoromethylsulfonyl)imide) that allows electrodeposition to be performed without a glove box. The electrochemistry of indium is thoroughly investigated and the drawbacks of using metal chloride precursors in Tf_2N-based electrolytes are highlighted using cyclic voltammetry and stripping experiments. Voltammograms revealed complex electrochemical behaviour and several cathodic and anodic signals that could be attributed to the formation of indium chloro complexes during the scan, due to changes in the concentration ratio $[Cl^-]/[In(III)]$ of interfacial species during the In(III) reduction reaction. A procedure for the electrodeposition of indium avoiding the use of the indium chloride precursor is then proposed. It offers an improved morphology of the electrodeposit and an increase in faradic yield from 33% to 85% compared to chloride-containing RTILs.

1. Introduction

Electrochemical deposition (ECD) of indium is of great interest for the production of thin-film semiconducting compounds such as InSb, InAs and $Cu(In,Ga)(S,Se)_2$, widely used in electronic and optoelectronic devices (e.g. detectors, lasers, photovoltaic devices and light-emitting diodes). ECD using indium-containing compounds in aqueous media has been extensively described in the literature [1,2]. It has been emphasised that deposition efficiency is limited by H^+ reduction.

Low melting-point ionic liquids or room-temperature ionic liquids (RTILs) are a new class of non-aqueous solvents considered as promising electrolytes for ECD of high quality thin films, since hydrogen is not evolved in these media [3–9]. They are liquid at or below room temperature and they display, in particular, high ionic conductivities and wide electrochemical windows [10]. Two main families of RTILs are commonly used for ECD purposes: halide-based compounds, also called first-generation RTILs, and second-generation "air- and water-stable" RTILs. Numerous examples of the use of first-generation RTILs for the ECD of single metals and alloys have been reported [11]. However, these chloroaluminate RTILs, combining aluminum chloride and dialkylimidazolium or dialkylpyridinium chloride, are highly hygroscopic and so have to be protected from moisture by working in a glove box. The use of RTILs has greatly increased since Riechel and Wilkes reported the first second-generation, air- and moisture-stable RTILs with either tetrafluoroborate or hexafluorophosphate as anions [12]. More recently, RTILs containing anions such as tri-fluoromethanesulfonate, bis(trifluoromethanesulfonyl)imide or tris(trifluoromethanesulfonyl)methide were synthesised and attracted attention because of their low viscosity, low hygroscopy and low reactivity towards moisture [13]. However, currently developed and commercialised electrolytes still have to be used in a dry atmosphere for ECD applications and so cannot be considered as viable electrolytes by the electroplating industry.

In addition, contrary to common belief, second generation RTILs are not "supersolvents" in which all kinds of materials can be easily dissolved. Due to the poor solvating power of

---

* Corresponding author. Tel.: +33 387 31 54 63; fax: +33 387 31 54 60.
** Corresponding author. Tel.: +33 479 75 88 59; fax: +33 479 75 86 74.
E-mail addresses: Youssouf.Traore1@etu.univ-savoie.fr (Y. Traore), sophie.legeai@univ-metz.fr (S. Legeai), sebastien.diliberto@univ-metz.fr (S. Diliberto), guilhem.arrachart@cea.fr (G. Arrachart), stephane.pellet-rostaing@cea.fr (S. Pellet-Rostaing), micheline.draye@univ-savoie.fr (M. Draye).
[1] Tel.: +33 479 75 88 98; fax: +33 479 75 86 74.
[2] ISE member is Sophie Legeai.
[3] Tel.: +33 387 31 54 63; fax: +33 387 31 54 60.
[4] Tel.: +33 466 79 15 68; fax: +33 466 79 76 11.
[5] Tel.: +33 466 33 93 08; fax: +33 466 79 76 11.
[6] Tel.: +33 479 75 88 59; fax: +33 479 75 86 74.

0013-4686/$ – see front matter © 2011 Elsevier Ltd. All rights reserved.
doi:10.1016/j.electacta.2011.09.085

these RTILs, composed of weakly coordinating anions, and to their moderate polarity, the solubility of inorganic ionic compounds in second-generation RTILs is actually very low unless chloride salts are used. However, the introduction of chloride ions in electroplating baths leads to undesirable chlorine gas evolution at the anode during ECD, makes the RTIL more hygroscopic and leads in some cases to complex electrochemical behaviour.

ECD of indium has recently been studied in an air- and moisture-stable RTIL, using a chloride salt as the indium cation source [14]. In these conditions, the In(III)/In(0) electrochemical system is far from simple, involving several reduction steps that are difficult to explain and require complex optimisation of ECD experimental parameters for high quality film synthesis. Also, in this earlier work, experiments were carried out in highly restrictive conditions, i.e. in a glove box with water and oxygen concentration levels below 1 ppm. This was because the electrolytic solutions used, consisting of a 1-butyl-1-methyl-pyrrolidinium bis(trifluoromethylsulfonyl)imide ($BMPTf_2N$) RTIL containing $InCl_3$ as the metal precursor, was too hygroscopic to perform the ECD experiments in ambient atmosphere.

In this paper, we report the electrodeposition of indium in a home-made weakly hygroscopic piperidinium ionic liquid (1-butyl-1-ethyl-piperidinium bis(trifluoromethylsulfonyl)imide: $BEPipTf_2N$) that allows electrodeposition to be performed without the need of a glove box. The synthesis and some physical and chemical properties of several piperidinium-based RTILs are first related. We then present a detailed study of the electrochemical behaviour of $InCl_3$ in the $BEPipTf_2N$ RTIL. The strong influence of chloride ions on the In(III)/In(0) electrochemical system and electrodeposition faradic yield is highlighted. We finally propose a procedure for the electrodeposition of indium in a chloride-free electrolyte to avoid the drawbacks of using a chloride-based precursor metal in a Tf_2N-based RTIL.

2. Experimental

Ionic liquids were prepared according to the published procedure of Triolo et al. [15], modified. Briefly, the nitrogen-based heterocycle yielded the corresponding ammonium salt by reaction with alkyl bromide. Bromide anion was then replaced by bis(trifluoromethylsulfonyl)imide (Tf_2N^-) by vigorous stirring of the alkylammonium bromide with an aqueous solution of lithium bis(trifluoromethylsulfonyl)imide ($LiTf_2N$, Solvionic, 99+%). After metathesis was complete the ionic liquid was extracted with dichloromethane (Sigma–Aldrich, >99.5%) and dried under reduced pressure for 3 h. Synthesised ionic liquids were characterised by nuclear magnetic resonance (NMR) analysis (Bruker Spectrospin DRX 300 MHz Ultrashield).

The density, viscosity and conductivity of RTILs were determined as a function of water content determined by Karl Fischer coulometric titration (Metrohm 831KF coulometer) using Hydranal 34843 Coulomat AG-H (Fluka) as titrant.

The density measurements were performed with a DSA 5000 thermo-regulated digital densimeter (Anton Paar). The apparatus measures densities using an oscillating U-tube with an accuracy of 0.00001 g/cm^3 and temperature controlled to within 0.001 °C.

All measurements were conducted at 20.005 ± 0.004 °C. The density was calculated from the quotient of the period of oscillations of the U-tube and the reference oscillator: density = $K_A \times Q^2 \times f_1 - K_B + f_2$, where K_A and K_B are constants specific to the apparatus, Q is the quotient of the period of oscillation of the U-tube divided by the period of oscillation of the reference oscillator and f_1 and f_2 are correction terms for temperature, viscosity and non-linearity.

All rheological measurements were performed using an AMVn automated microviscosimeter (Anton Paar). The apparatus measures viscosities in a 0.3–2500 mPa s range using the rolling ball/falling ball principle, which consists in measuring ball rolling time in a diagonally mounted glass capillary filled with the sample. Ball rolling time was measured with an accuracy of 0.002 s at a temperature controlled to within 0.001 °C.

All measurements were made at 20.00 °C with a 70° inclination angle of the capillary, and the dynamic viscosity η was calculated using the formula $\eta = K_1 \times (\rho_K - \rho_P) \times t_1$, where K_1 is the calibration constant of the measuring system, ρ_K is the ball density, ρ_P is the density of the measured sample and t_1 is the ball rolling time.

Conductivities of RTILs were measured using a Tacussel Electronique CDRV62 conductimeter/resistivitimeter with a platinum 2-electrode cell (Materials Mates). The cell was calibrated with 5×10^{-3} to 3.3×10^{-2} KCl solutions, and the data were recorded at a frequency of 62 Hz.

The solubility of water in the RTILs was determined by Karl Fischer coulometric titration after RTIL contact with distilled water. The water content of water-saturated RTILs in equilibrium with water was measured by mixing water and each RTIL for 24 h. The two-phase system was then centrifuged and the RTIL water content was measured.

Electrochemical experiments were carried out using a PGP201 potentiostat (Radiometer Copenhagen) and a Tacussel Electronique potentiostat (101T and PJT24-1). Before electrochemical experiments the electrolytic solution was de-aerated and dried down to a water content below 50 ppm by dry argon bubbling. In(III) solutions were prepared either by dissolution of $InCl_3 \cdot 4H_2O$ (Sigma–Aldrich, 97%) or by electrochemical potentiostatic dissolution of a soluble indium anode (Alfa Aesar, 99.99%) in the selected ionic liquid at ambient temperature. It appeared that $InCl_3 \cdot 4H_2O$ salt was readily soluble in the ionic liquid and concentration values up to 0.25 M were easily achieved. All experiments were performed at 60 °C to lower RTIL viscosity and increase mass transport. Electroanalytical studies were carried out using a conventional three-electrode electrochemical cell, with a platinum disk (19.6 mm^2) as working electrode, glassy carbon as counter electrode and an AgCl-covered Ag wire (Alfa Aesar 99.999%) as pseudo-reference electrode. This latter was separated from the bulk solution by a salt bridge, containing only the RTIL electrolyte, in order to avoid the variations of its potential as a function of Cl^- concentration in the bulk. This pseudo-reference electrode was prepared by chemical oxidation of an Ag wire in a $FeCl_3$ aqueous solution, and carefully dried before use. Square platinum plates (Goodfellow, Lille, France, 99.99%, area 25.0 mm^2) were used as substrates for the electrodeposition of indium. Electrodeposition was achieved by controlled potential electrolysis in steadily stirred $BEPipTf_2N$ containing In(III). Before the electrochemical experiments were carried out, the working electrode was polished with SiC abrasive papers and 1 μm diamond paste, and then soaked in deionised water and acetone. After electrodeposition, the indium-coated square platinum plate electrodes were immediately transferred from the electrodepositing baths into acetone to remove residual RTIL.

The surface morphology and grain size of the deposits were determined using a scanning electron microscope (FEG-SEM) (Philips XL30), equipped with an energy dispersive spectrometry (EDS) detector. Structural characterisations were conducted by X-ray diffraction (XRD) using a Bruker diffractometer (D8 Advance, Cu $K\alpha_1$ radiation).

ECD faradic yields were determined by atomic absorption spectrometry (Varian AA240FS) after chemical dissolution of the deposits in 3 M HNO_3.

Table 1
Physical and chemical properties of bis(trifluoromethylsulfonyl)imide (Tf_2N)-based RTILs tested in this study.

RTIL cation	Density ($g\,cm^{-3}$) 20 °C	Electro chemical window (V)	Cathodic stability (V *vs.* AgCl/Ag)	Conductivity ($mS\,cm^{-1}$) 25 °C (*ppm H_2O*)	Dynamic viscosity (mPa s) 20 °C (*ppm H_2O*)	Kinematic viscosity ($mm^2\,s^{-1}$) 20 °C (*ppm H_2O*)	H_2O sat (ppm)
BMI[a]	1.43918 (*2215*)	4.3	−1.8	3.3 (*312*)	58.7 (*2215*)	40.8 (*2215*)	14,990
	1.429 [10]	3.5 [17]		4.0 [18]	52 [18]		
				3.9 [10]			
BMP[b]	1.39723 (*537*)	5.1	−2.4	2.6 (*286*)	97.8 (*537*)	70.0 (*537*)	13,123
	1.41 [10]	4.0 [20]		2.2 [10]	85 [18]		11,700 [21]
	1.393 [16]				76 [16]		
BMPip[c]	1.38342 (*653*)	4.8	−2.2	0.93 (*358*)	248.7 (*653*)	179.8 (*653*)	10,115
	1.378 [16]			1.1 [16]	200 [21]	182 [16]	10,050 [21]
				1.3 [21]			
MOPip[d]	1.28443 (*781*)	5.1	−2.4	0.40 (*315*)	406.9 (*781*)	316.8 (*781*)	7961
							6590 [21]
BEPip[e]	1.36623 (*415*)	4.9	−2.4	0.82 (*150*)	290 (*415*)	212.4 (*415*)	10,289
EOPip[f]	1.27426 (*721*)	5.3	−2.5	0.34 (*245*)	423.3 (*721*)	332.2 (*721*)	7157

[a] 1-Butyl-3-methylimidazolium.
[b] 1-Butyl-1-methyl-pyrrolidinium.
[c] 1-Butyl-1-methyl-piperidinium.
[d] 1-Methyl-1-octyl-piperidinium.
[e] 1-Butyl-1-ethyl-piperidinium.
[f] 1-Ethyl-1-octyl-piperidinium.

3. Results and discussion

3.1. Physicochemical properties of 1,1-dialkyl-$PipTf_2N$ RTILs

Few literature reports have focused on piperidinium-based RTILs because of their low commercial availability [16]. However, their physical and chemical properties can be compared to more extensively used pyrrolidinium- and imidazolium-based RTILs [10,16–21].

The density, electrochemical stability, conductivity and viscosity of several 1,1-dialkyl-$PipTf_2N$ RTILs, together with the solubility of water in these solvents, are presented in Table 1 and compared with results obtained with imidazolium and pyrrolidinium-based RTILs (our results and literature data). As the density, conductivity and viscosity of ionic liquids can be affected by water impurities, values are reported in Table 1 along with corresponding RTIL water content in italics.

The physical and chemical properties determined in this work were in close agreement with literature data when available. Results obtained for cathodic stability cannot be compared with literature data as the latter refer to other reference electrode devices. Cathodic stability and water solubility values obtained in this work followed the order $BMITf_2N < BMPyrrolTf_2N \sim BMPipTf_2N \sim BEPipTf_2N \sim MOPipTf_2N \sim < EOPipTf_2N$. Hence all the piperidinium-based RTILs tested presented a wider electrochemical window and were less hygroscopic than the other RTILs under consideration. It is commonly accepted that RTILs based on saturated-ring cations, such as pyrrolidinium or piperidinium cations, present higher cathodic stability than unsaturated-ring cations, such as imidazolium or pyridinium-based cations, as a double bond is more vulnerable to electrochemical reaction than a saturated one. Thus, among nitrogen-based RTILs, those containing four coordinate nitrogens (ammonium, pyrrolidinium, piperidinium, morpholinium) have the highest cathodic stabilities [10]. It has also been suggested that 1,3-disubstituted imidazolium cations show a poor cathodic stability because of the presence of an acidic proton at the C-2 position that undergoes a reduction to molecular hydrogen [10]. It is also well established that an increase in the length of the alkyl side chain leads to higher cathodic stability of the cation [10]. However, the piperidinium ring leads to more viscous and consequently less conductive RTILs than similar imidazolium or pyrrolidinium compounds. Finally, increasing cation alkyl chain length also leads to a decrease in the conductivity of RTILs, mainly due to an increase in viscosity, as commonly observed [10].

The best compromise between cathodic stability, conductivity and hygroscopic character appeared to be $BEPipTf_2N$, and so this RTIL was selected for subsequent studies. Table 1 shows $BEPipTf_2N$ to be hydrophobic enough to make a glove box unnecessary.

3.2. Electrochemical behaviour of $InCl_3$-containing electrolytes

Fig. 1 shows a typical cyclic voltammogram on a platinum working electrode in $BEPipTf_2N$ containing 0.1 M $InCl_3$. The cyclic voltammogram is quite complex: several cathodic (c_1–c_5) and anodic (a_1–a_5) processes can be observed over the full potential range tested. To elucidate the complete voltammogram, several experiments were undertaken by cyclic voltammetry and potentiostatic deposition followed by either anodic stripping or XRD/SEM-EDS analysis of corresponding deposits.

3.2.1. Electrodeposition of indium on square platinum plates and surface analysis of potentiostatic deposits

One-hour potentiostatic deposition experiments were carried out for several potential values, corresponding to c_1–c_5 peaks on square platinum electrodes. XRD patterns confirm the presence of indium metal for potential values lower than 200 mV *vs.* (AgCl/Ag).

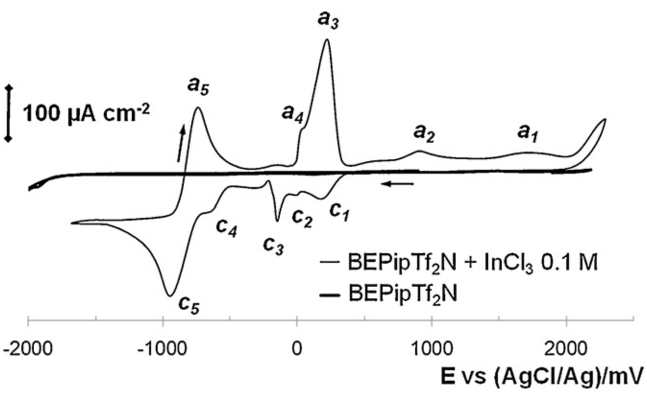

Fig. 1. Cyclic voltammograms recorded on platinum in $BEPipTf_2N$. Scan rate 5 mV/s. $T = 60\,°C$.

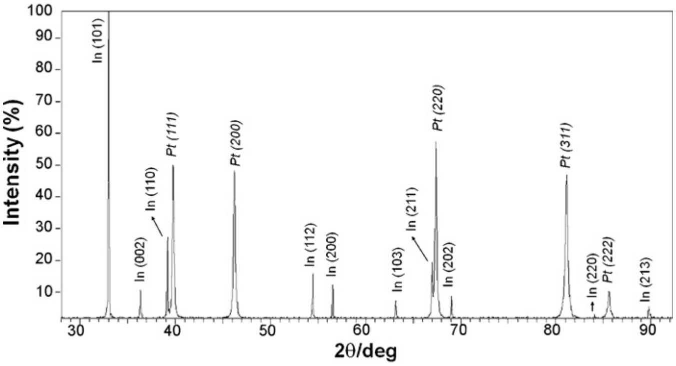

Fig. 2. XRD pattern of an indium deposit on a platinum substrate. BEPipTf$_2$N + InCl$_3$ 0.1 M. E_{dep} = −920 mV *vs.* (AgCl/Ag), t_{dep} = 1 h. T = 60 °C.

Fig. 2 shows a typical XRD pattern of In(0) deposits obtained at E_{dep} = −920 mV *vs.* (AgCl/Ag).

SEM-EDS analysis revealed that c$_1$, c$_2$ and c$_4$ applied potentials led to only small amounts of In(0) on the electrode and that only the c$_5$ peak corresponded to bulk deposition. This had already been observed by Zein el Abedin et al. [14], who suggested that the c$_1$–c$_4$ peaks might correspond to multiple UPD/Pt-alloying processes; however, this hypothesis was neither confirmed nor refuted by detailed experimental electrochemical investigations. Also, the absence of indium metal deposition between c$_3$ and c$_4$ is quite surprising. This behaviour is markedly different from that previously reported. Very simple voltammetric curves with only single electrochemical signals were recorded using other substrates (Mo [22,23], glassy carbon [24–26], Hg [1,27], In [1,28]) and other solvents (high temperature molten salts [23,24,28], RTILs [22,25] or aqueous medium [1,27]).

3.2.2. *Detailed voltammetric study of In(III) in BEPipTf$_2$N*

To gain a deeper understanding of the In(III)/In(0) electrochemical system in our electrolyte, a detailed voltammetric study was undertaken. First, to identify possible alloying processes with platinum substrate, the voltammogram obtained on platinum was compared with a cyclic voltammogram run using a stainless steel working electrode (Fig. 3). With stainless steel, anodic potential windows are limited by electrode oxidation and so peaks a$_1$ and a$_2$ could not be studied.

Cyclic voltammograms presented roughly the same characteristics using either electrode, except for the c$_1$ signal, which was not observed on steel. This observation suggests that the c$_1$ signal recorded on the platinum substrate could be due to an In–Pt alloying process.

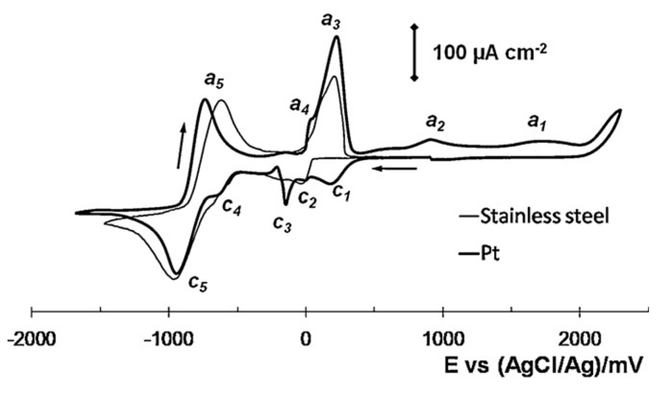

Fig. 3. Cyclic voltammograms recorded in BEPipTf$_2$N containing 0.1 M InCl$_3$ on platinum and stainless steel. Scan rate 5 mV/s. T = 60 °C.

Voltammetric experiments with ranging cathodic reversal potentials were then carried out using the platinum electrode, in order to study the other electrochemical signals (Fig. 4b–f). The complete voltammogram is shown in Fig. 4a.

When the scan was reversed just after peak c_1 at +50 mV *vs.* (AgCl/Ag) (Fig. 4e), two oxidation peaks, a$_1$ and a$_2$, were observed during the return scan. Previous results (Fig. 2) suggest that these anodic peaks may result from an In–Pt alloying process occurring at c$_1$. To distinguish between UPD and In–Pt alloying, another cyclic voltammetry experiment was undertaken without reaching the potential for oxidative stripping during the return scan. As can be observed in Fig. 4f, the successive cycles are quite identical, showing that the alloying hypothesis is the most plausible. If it were UPD, there should not be any observable reductive charge during the second scan, since the surface would be already covered with an In monolayer.

When cathodic potentials were decreased to −100 mV *vs.* (AgCl/Ag), a new anodic peak a$_3$ appeared during the reverse scan, the intensity of which increased with decreasing reversal potential (Fig. 4e). The electrochemical signal c$_2$ may thus be due to the deposition of indium metal. Complementary potentiostatic experiments were undertaken at −100 mV *vs.* (AgCl/Ag) for several deposition times, followed by anodic stripping using linear voltammetry (Fig. 5a). The results obtained confirmed the hypothesis that c$_2$ corresponded to In(0) deposition and a$_3$ corresponded to elemental indium stripping. One can notice that a$_1$ peak potential is more anodic than a$_3$ peak potential, according to In–Pt alloying previous hypothesis, as In–Pt alloy needs higher positive potential than In metal to draw it away from the Pt matrix.

Surprisingly, by further decreasing the reversal potential down to −500 mV *vs.* (AgCl/Ag), the intensity of the a$_3$ anodic peak decreased (Fig. 4d). Simultaneously, a$_1$ increased, with potential switching becoming more cathodic. Potentiostatic deposition at the c$_3$ peak potential, followed by anodic stripping, was also performed for several deposition times. The results obtained confirmed the decrease in the a$_3$ anodic peak and the increase in a$_1$ with increasing deposition time (Fig. 5b). We also note the shape of the c$_3$ peak, characteristic of a surface reaction limited by a finite amount of matter, suggesting that previously deposited In(0) may undergo an electrochemical transformation (surface rearrangement, second In–Pt alloying step, etc.). At the present time, none of the experiments performed favour any hypothesis for the electrochemical reaction corresponding to the c$_3$ cathodic peak.

Fig. 4b and c show that the c$_5$ cathodic peak previously attributed to bulk deposition of In(0) by XRD analysis is related to three anodic stripping peaks: a$_3$, a$_4$ and a$_5$. The link between c$_5$ and a$_3$ is in agreement with previous observations attributing the a$_3$ signal to In(0) stripping (Fig. 4e). As shown in Fig. 4b, the a$_3$ peak was observed only for a switching potential lower than −920 mV *vs.* (AgCl/Ag), and its peak current then increased as the switching potential became more cathodic. Conversely, a$_4$ and a$_5$ peak currents reached constant values for potentials lower than −1200 mV *vs.* (AgCl/Ag).

To confirm voltammetric results, potentiostatic experiments were undertaken at the c$_5$ peak potential for increasing deposition times, followed by anodic stripping using linear voltammetry. The results obtained are presented in Fig. 6a.

We see that only the a$_3$ peak grew significantly with deposition time, indicating that the a$_3$ signal could be related to the anodic “bulk” dissolution of previously deposited In(0). Fig. 6b presents anodic charges Qa$_3$, Qa$_4$ and Qa$_5$, corresponding respectively to peaks a$_3$, a$_4$ and a$_5$, together with $Q_{a\ total} = Qa_3 + Qa_4 + Qa_5$, as a function of cathodic charge Q_c related to potentiostatic deposition.

$Q_{a\ total}$ grew linearly with Q_c, indicating that the three anodic peaks under consideration may be related to anodic dissolution of In(0) deposited during the potentiostatic step. Considering anodic

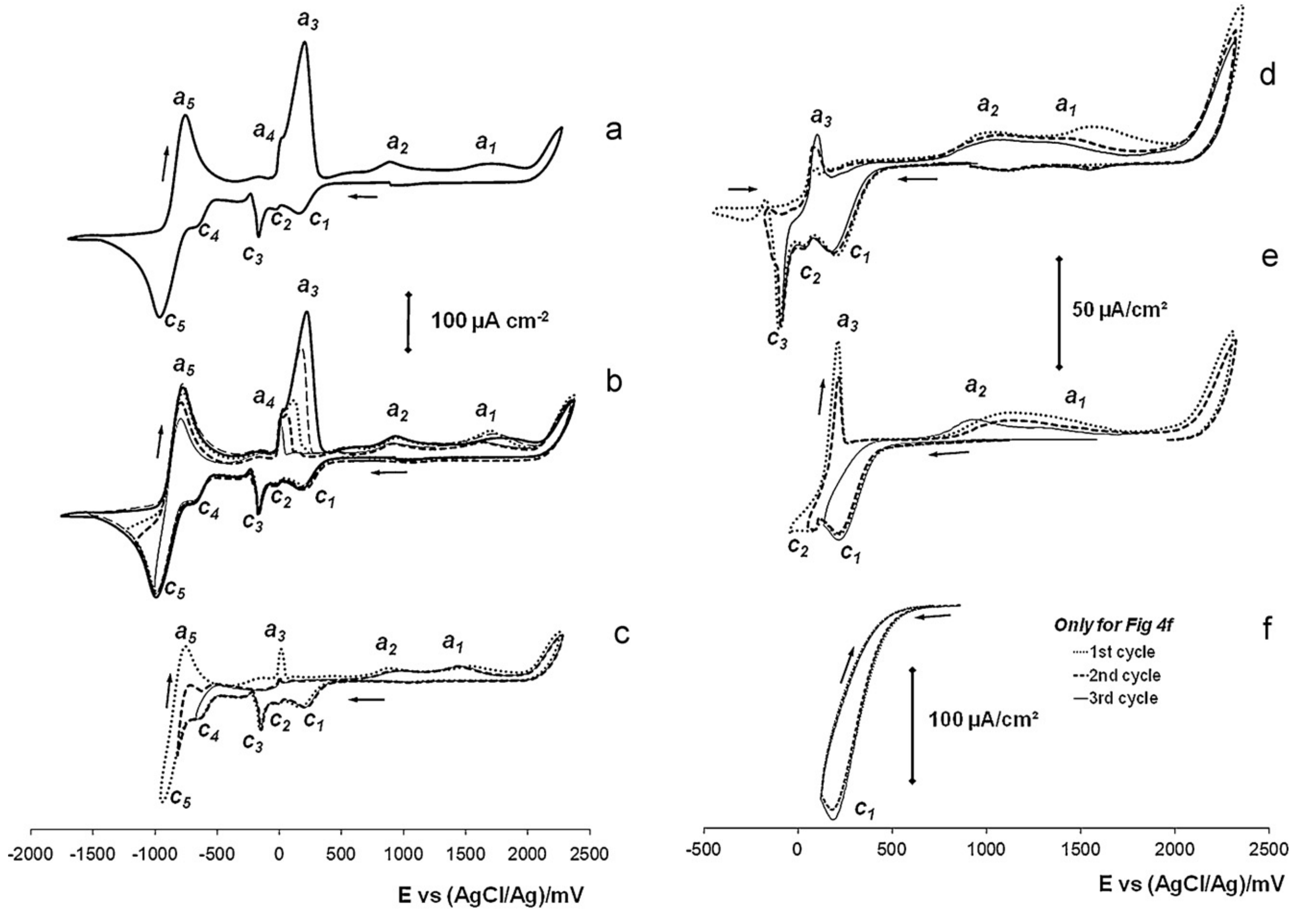

Fig. 4. Cyclic voltammograms recorded on platinum in BEPipTf$_2$N containing 0.1 M InCl$_3$ with different reversal potentials. Scan rate 5 mV/s. T = 60 °C.

charges Qa_3, Qa_4 and Qa_5 separately, we found that Qa_3 increased linearly with Q_c for deposition times longer than 2 min (21.2 mC curve in Fig. 6a), whereas Qa_4 and Qa_5 remained constant in the same range of deposition time. By contrast, for deposition times shorter than 2 min, the opposite behaviour was observed: Qa_4 and Qa_5 increased linearly with Q_c, whereas Qa_3 increased only slowly (see inset Fig. 6b). Hence the a$_5$ and a$_4$ signals may be related to mass transport limited processes associated with indium metal dissolution. A possible hypothesis is that the a$_4$ and a$_5$ signals are related to the formation of species limited by chloride ion mass transport, such as $\mathrm{In}_x\mathrm{Cl}_y{}^{3x-y}$ complexes. These electrochemical processes cannot be observed when using chloride-based RTILs [22,25] or high temperature molten salts [23,24,28] in which chloride mass transport is not limiting, as chloride ions are not present as solutes but as part of the solvent. It must be kept in mind that RTILs are viscous media in which mass transport is very slow. The hypothesis of a limitation by chloride ion mass transport is also supported by the diffusional shape of the a$_5$ signal. The same hypothesis could also explain why c$_2$ and c$_5$ cathodic signals were both related to In(0) deposition and could correspond to the reduction of several In(III)-based species.

3.3. Influence of chloride ions on In(III)/In(0) electrochemical behaviour

3.3.1. In(III) electrochemical behaviour in a chloride-free electrolyte

To test the previous hypothesis concerning the influence of Cl$^-$ ions on In(III) electrochemical behaviour, a chloride-free electrolytic solution was studied. In(III) ions were introduced into the RTIL by potentiostatic oxidation of a soluble indium anode. The counter electrode was isolated in a salt bridge to prevent electrolyte degradation. The concentration of In(III) species was calculated by the mass loss of the soluble anode. A typical cyclic voltammogram of the resulting solution is given in Fig. 7.

A very simple voltammogram was obtained compared with those previously recorded using InCl$_3$. A single electrochemical system was observed, with a nucleation loop at −70 mV *vs.* (AgCl/Ag), characteristic of a metal deposition process. This voltammogram is very similar to the one obtained using InCl$_3$ in chloride-based electrolytes [22–25,28] and is characteristic of a single species in solution. In chloride-based RTIL, In(III) occurs solely as $\mathrm{InCl_5}^{2-}$. In our case, In(III) may occur as In^{3+} or $\mathrm{In}_x(\mathrm{Tf_2N})_y{}^{3x-y}$.

XRD/SEM-EDS analysis of potentiostatic deposits confirmed the presence of indium metal for deposition potential values lower than −80 mV *vs.* (AgCl/Ag).

3.3.2. Influence of Cl$^-$ concentration on the electrochemical behaviour of In(III) in BEPipTf$_2$N

The influence of Cl$^-$ concentration on the electrochemical behaviour of In(III) was studied by adding increasing amounts of a chloride-based RTIL to the previously prepared chloride-free In(III) solution. Fig. 8a–d presents the corresponding voltammograms recorded at the platinum electrode.

We see that as soon as Cl$^-$ ions were introduced into the In(III) solution, a second electrochemical system appeared, characterised by a cathodic peak at −850 mV *vs.* (AgCl/Ag) and a corresponding anodic peak at −800 mV *vs.* (AgCl/Ag) (Fig. 8a). This electrochemical system shifted progressively towards more cathodic potential values as the Cl$^-$ concentration increased (Fig. 8b

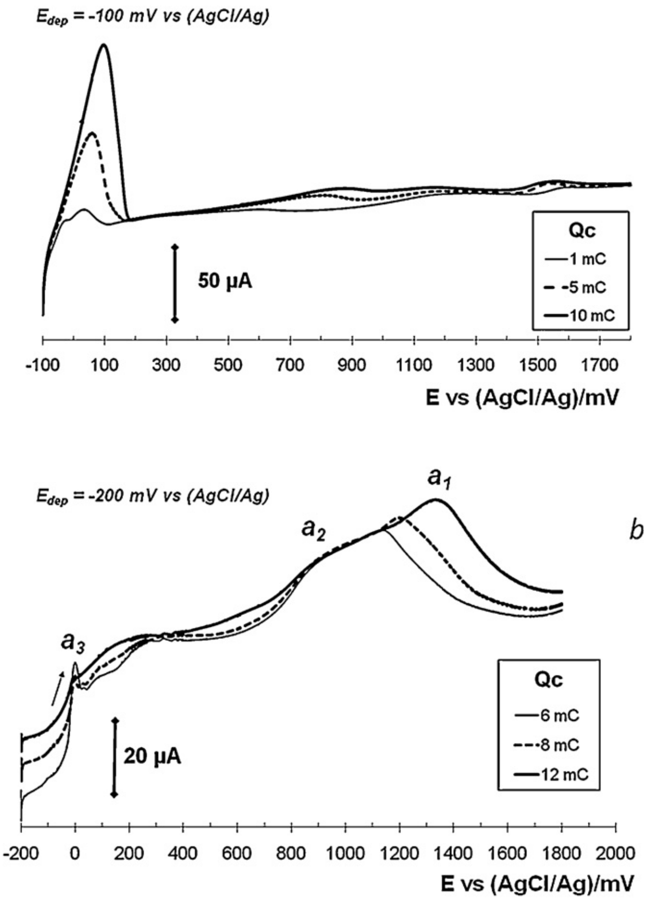

Fig. 5. Voltammograms recorded during anodic stripping of indium in BEPipTf$_2$N containing 0.1 M InCl$_3$, for different deposition charge values. Platinum substrate. Scan rate 5 mV/s. $T = 60\,^\circ$C. (a) $E_{dep} = -100$ mV *vs.* (AgCl/Ag) and (b) $E_{dep} = -200$ mV *vs.* (AgCl/Ag).

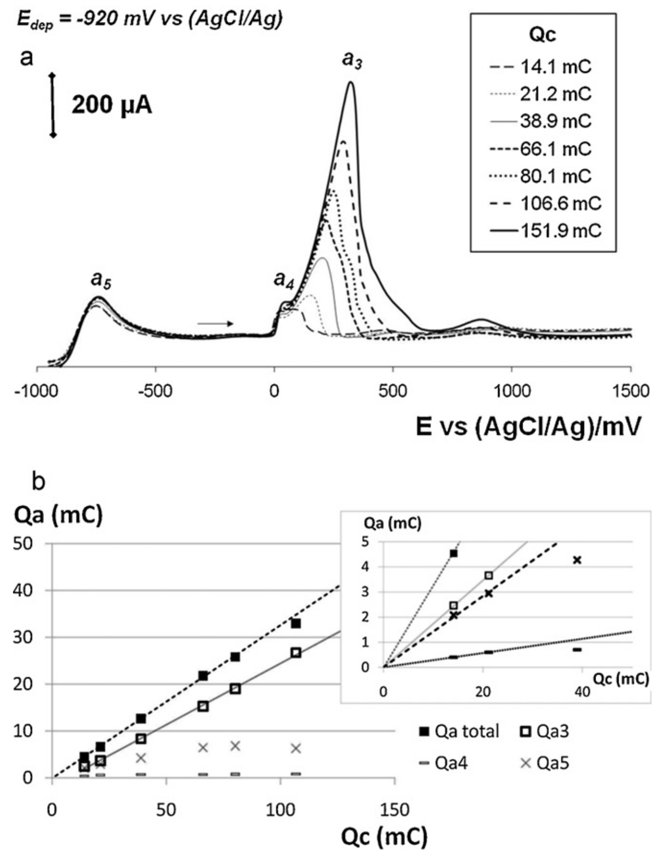

Fig. 6. (a) Voltammograms recorded during anodic stripping of indium in BEPipTf$_2$N containing 0.1 M InCl$_3$, for different deposition charge values. Platinum substrate. Scan rate 5 mV/s. $T = 60\,^\circ$C. $E_{dep} = -920$ mV *vs.* (AgCl/Ag). (b) Anodic charges corresponding to potentiodynamic stripping of indium (voltammograms presented in Fig. 6a) as a function of cathodic charge related to potentiostatic deposition. BEPipTf$_2$N containing 0.1 M InCl$_3$. Platinum substrate. $T = 60\,^\circ$C. $E_{dep} = -920$ mV *vs.* (AgCl/Ag). Inset: zoom representing shortest deposition times.

and c). Corresponding peak currents increased with Cl$^-$ concentration and we can observe the simultaneous decrease in peak currents related to the "free" In(III)/In(0) system. This behaviour reveals the presence of indium chloride species In$_x$Cl$_y$$^{3x-y}$. By overlaying the cyclic voltammogram recorded in an InCl$_3$-containing electrolyte of identical In(III) concentration, it appeared that the electrochemical signals c$_5$/a$_5$ corresponded to an In$_x$Cl$_y$$^{3x-y}$/In(0) electrochemical system (Fig. 8d). We can also conclude from these experiments that the electrochemical signals c$_2$/a$_3$ corresponded to the "free" In(III)/In(0) system. The exact formula of the chloride complex could not be determined, as cyclic voltammograms are affected by the progressive increase in electrolyte viscosity with chloride-based RTIL addition. This could also explain why the voltammogram recorded for a [Cl$^-$]/[In(III)] ratio of 3 did not match, in terms of peak intensities, the voltammogram corresponding to the InCl$_3$-containing electrolyte.

These experiments highlight the formation of indium chloride complex species during a cyclic voltammetry experiment. This occurrence can be explained by the changes in interfacial relative concentrations of In(III) and Cl$^-$ species during the cathodic/anodic scans, due to In(III) consumption/formation. As the cathodic scan progresses, In(0) deposition occurs and the interfacial ratio [Cl$^-$]/[In(III)] increases, leading to the formation of In$_x$Cl$_y$$^{3x-y}$ species that are reduced at more cathodic potentials. At the beginning of the forward scan, the ratio [Cl$^-$]/[In(III)] is high and the stripping of previously deposited In(0) leads first to the formation of an indium chloride complex. The interfacial ratio [Cl$^-$]/[In(III)] then decreases and the In(0) stripping reaction leads to the formation of "free" In(III). This hypothesis was supported by deposition/stripping experiments (Fig. 6): as the amount of deposited In(0) increased, the a$_5$ peak reached a constant value related to the limiting mass transport of Cl$^-$ species, whereas the a$_3$ peak increased.

These multiple electrochemical processes are due to the use of a Tf$_2$N-based electrolyte associated with a metal chloride-based precursor. The same electrochemical behaviour may be observed with any metal ion able to form complex species with the counter-anion of its metal precursor salt. It has already been observed for SeCl$_4$-containing RTILs: a single electrochemical system was observed by

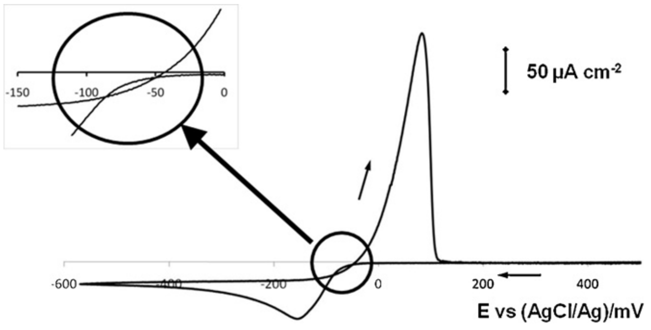

Fig. 7. Cyclic voltammogram of a 1.87×10^{-2} M In(III) solution of chloride-free BEPipTf$_2$N. Scan rate 5 mV/s. $T = 60\,^\circ$C. Platinum substrate.

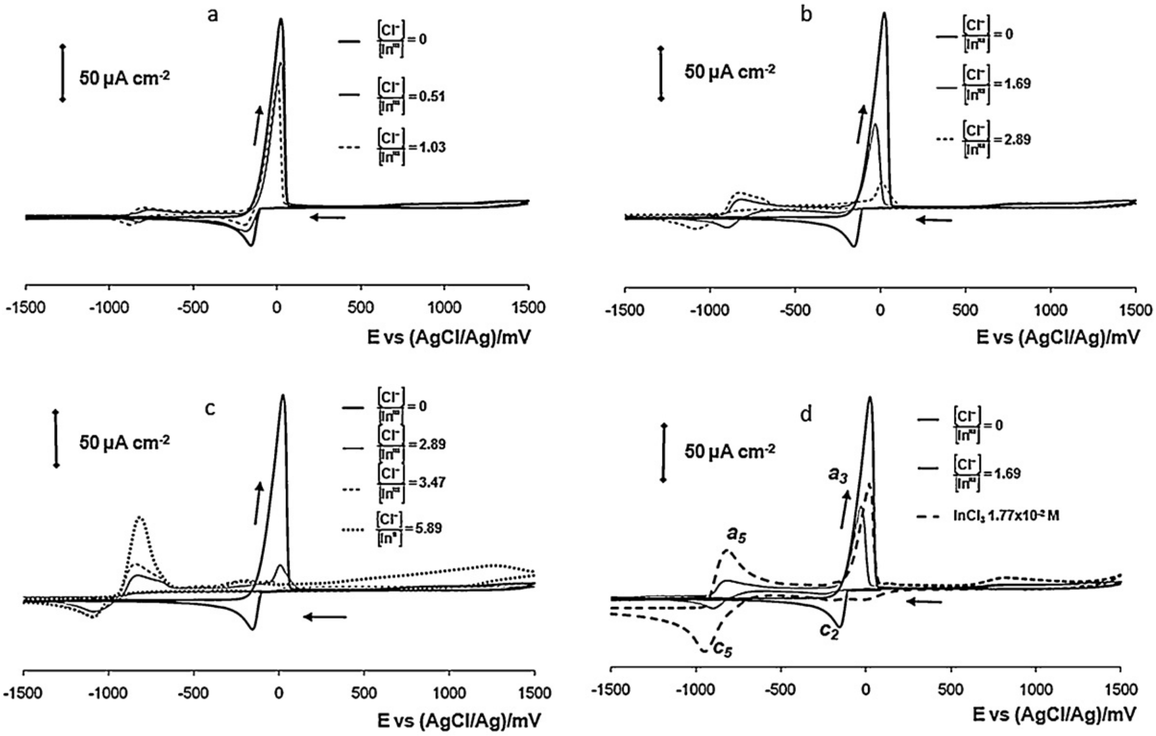

Fig. 8. Cyclic voltammograms of a 1.87×10^{-2} M In(III)-containing BEPipTf$_2$N solution, recorded for different values of the [Cl$^-$]/[In(III)] ratio. Scan rate 5 mV/s. T = 60 °C. Platinum substrate.

Dale et al. [22] in a chloride-based RTIL, while Zein el Abedin et al. [14] recorded a very complex voltammogram in a Tf$_2$N-based RTIL.

More experiments will be necessary to completely understand the electrochemical behaviour of InCl$_3$ containing Tf$_2$N-based RTIL, as some electrochemical signals cannot be clearly explained by mass transport phenomena. Recently, Fu et al. highlighted, by the mean of STM studies, the adsorption of molecular chloride metallic species (BiCl$_3$, SbCl$_3$, SbBr$_3$) on working electrode surface that lead to the UPD of metallic monolayers [29]. The same phenomenon could be responsible of the non-attributed electrochemical signals recorded in this work using InCl$_3$ as precursors, as these signals were not observed in the chloride-free RTIL.

3.4. Electrochemical deposition of indium

Indium electrodeposition was performed under potentiostatic conditions using both InCl$_3$-containing electrolytes and chloride-free electrolytes containing In(III) species introduced by anodic dissolution of an indium anode. Using InCl$_3$-containing RTILs, deposition experiments were conducted only in the potential range corresponding to the bulk deposition of In(0) (around the c$_5$ signal). In both cases, the following deposition potential values were tested: $E_{1/2}$, E_{peak} and ($E_{\text{peak}} - 100$ mV). Each deposit was analysed by XRD and SEM-EDS. The faradic yield of each electrodeposition process was evaluated by AAS after chemical dissolution of the deposit in 3 M HNO$_3$.

Adherent, homogeneous and covering deposits were obtained for all the experimental conditions tested (Fig. 9).

For each deposit, XRD analysis confirmed the presence of indium metal on the platinum substrate. Average faradic yields obtained for each applied potential are presented in Table 2.

The highest faradic yields were obtained in both electrolytes for E_{peak} deposition potential. We note in Table 2 that faradic yields obtained using the chloride-free electrolyte were much higher than

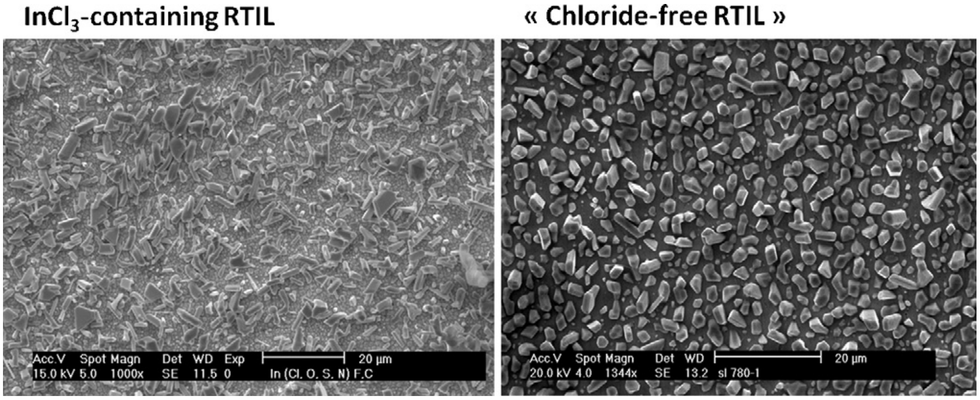

Fig. 9. Typical SEM micrographs of indium deposits obtained in BEPipTf$_2$N. Platinum substrate. 60 min deposition. (a) BEPipTf$_2$N + InCl$_3$ 9.22×10^{-2} M. $E_{\text{dep}} = -920$ mV *vs.* (AgCl/Ag), b: chloride-free BEPipTf$_2$N. $E_{\text{dep}} = -140$ mV *vs.* (AgCl/Ag). [In(III)] = 7.31×10^{-2} M.

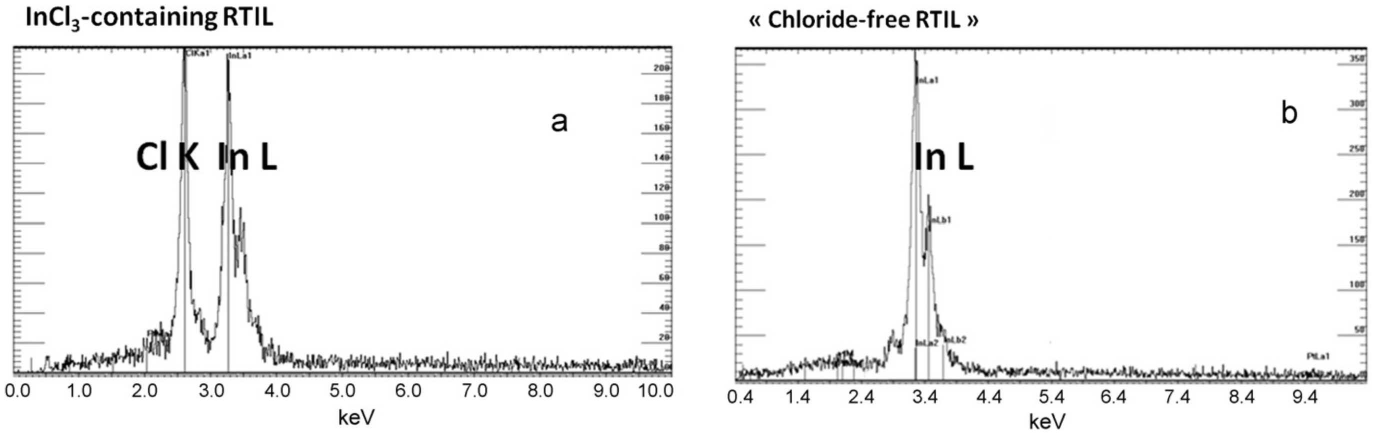

Fig. 10. EDS analysis of indium deposits obtained in BEPipTf$_2$N. Platinum substrate. 60 min deposition (sample presented in Fig. 9). (a) BEPipTf$_2$N + InCl$_3$ 9.22×10^{-2} M. $E_{dep} = -920$ mV *vs.* (AgCl/Ag) and (b) chloride-free BEPipTf$_2$N. $E_{dep} = -140$ mV *vs.* (AgCl/Ag). [In(III)] = 7.31×10^{-2} M.

Table 2
Electrodeposition of indium on platinum in BEPipTf$_2$N: average faradic yields.

Metallic precursor	E_{dep} (mV *vs.* AgCl/Ag)	Yield (%)
InCl$_3$	−810 ($E_{1/2}$)	33.7
	−920 (E_{peak})	35.6
	−1080	32.2
In anode	−125 ($E_{1/2}$)	65.5
	−140 (E_{peak})	85.5
	−340	77.2

those obtained with the InCl$_3$-containing solution whatever the deposition potential applied. This effect can thus be attributed to the presence of Cl$^-$ ions in the electrolyte. These low faradic yields could be related to a secondary electrochemical reaction, the non-elucidated cathodic process occurring between c$_3$ and c$_4$, which leads to a consumption of indium metal simultaneously with its bulk deposition.

In addition, the changes in the interfacial ratio [Cl$^-$]/[In(III)] during deposition process, which leads to the shift of the In(0) deposition potential towards more cathodic values as the ratio [Cl$^-$]/[In(III)] increases (Fig. 8), could explain the improved morphology obtained in chloride-free electrolytes compared with InCl$_3$-containing solutions (Fig. 9).

Finally, EDS spectra (Fig. 10) reveal the presence of Cl on the deposits obtained in InCl$_3$-containing RTILs, possibly due to chloride adsorption on the electrode surface [29], the inclusion of chloride ions in the deposits during electrodeposition process or the formation of indium chloride species, as shown by Carpenter and Verbrugge [30]. These species could also be involved in non-identified electrochemical signals on the cyclic voltammogram of InCl$_3$-containing electrolytes (Fig. 1).

4. Conclusion

In the first part of this paper, we have presented the synthesis and some physical and chemical properties of a new weakly hygroscopic RTIL, 1-butyl-1-ethyl-piperidinium bis(trifluoromethylsulfonyl)imide (BEPipTf$_2$N), which enabled us to perform In(0) ECD without needing a glove box.

The analytical study in the second part reveals the strong influence of Cl$^-$ ions on the electrochemical behaviour of In(III). The formation of indium chloride complexes due to the changes in the concentration ratio [Cl$^-$]/[In(III)] of interfacial species during the In(III) reduction reaction is highlighted. The formation of these multiple indium-based species results in very complex voltammograms and makes ECD experimental conditions very difficult to optimise. Another consequence, which is presented in the third part of this paper, is the marked decrease in the faradic yield corresponding to In(III) ECD in the presence of Cl$^-$ ions. EDS analysis also reveals the presence of chlorine, which may either be included in the deposits or correspond to non-metallic indium-based compounds.

This study shows that great care is needed when using metal chloride salts in Tf$_2$N-based RTIL, especially for metal ions that form stable chloride complexes, for example In(III), Se(IV), Te(IV) or Ga(III). These RTILs are very popular in the electrochemical community because of their low viscosity, their high electrochemical stability and their weakly hygroscopic character. However, the use of a Tf$_2$N-based electrolyte associated with a metal chloride-based precursor can lead to complex electrochemical systems and so be prejudicial to ECD processes.

Acknowledgements

The authors thank the 'Cluster Chimie' of the 'Région Rhône-Alpes' and the GNR CNRS SPDC2 for their financial support.

References

[1] R. Piercy, N.A. Hampson, J. Appl. Electrochem. 5 (1975) 15.
[2] S. Taunier, J. Sicx-Kurdi, P.P. Grand, A. Chomont, O. Ramdani, L. Parissi, P. Panheleux, N. Naghavi, C. Hubert, M. Ben-Farah, J.P. Fauvarque, J. Connolly, O. Roussel, P. Mogensen, E. Mahe, J.F. Guillemoles, D. Lincot, O. Kerrec, Thin Solid Films 480 (2005) 526.
[3] Q. Liao, W.R. Pitner, G. Stewart, C.L. Hussey, G.R. Stafford, J. Electrochem. Soc. 144 (1997) 936.
[4] E.G.-S. Jeng, I.W. Sun, J. Electrochem. Soc. 144 (1997) 2369.
[5] S.-I. Hsiu, I.W. Sun, J. Appl. Electrochem. 34 (2004) 1057.
[6] Y. Katayama, S. Dan, T. Miura, T. Kishi, J. Electrochem. Soc. 148 (2001) C102.
[7] T. Tsuda, T. Nohira, Y. Ito, Electrochim. Acta 46 (2001) 1891.
[8] E.R. Schreiter, J.E. Stevens, M.F. Ortwerth, R.G. Freema, Inorg. Chem. 38 (1999) 3935.
[9] W.R. Pitner, C.L. Hussey, J. Electrochem. Soc. 144 (1997) 3095.
[10] J.L. Anthony, J.F. Bennecke, J.D. Holbrey, E.J. Maginn, R.A. Mantz, R.D. Rogers, P.C. Trulove, A.E. Visser, T. Welton, in: P. Wasserscheid, T. Welton (Eds.), Ionic Liquids in Synthesis, Wiley-VCH Verlag GmbH & Co., 2002 (Chapter 3).
[11] G.R. Stafford, C.L. Hussey, in: R.C. Alkire, D.M. Kolb (Eds.), Advances in Electrochemical Science and Engineering, vol. 7, Wiley-VCH, Weinheim, 2001 (Chapter 6).
[12] T.L. Riechel, J.S. Wilkes, J. Electrochem. Soc. 139 (1992) 977.
[13] M. Gazlinski, A. Lewandowski, I. Stepniak, Electrochim. Acta 51 (2006) 5567.
[14] S. Zein el Abedin, A.Y. Saad, H.K. Farag, N. Borisenko, Q.X. Liu, F. Endres, Electrochim. Acta 52 (2007) 2746.
[15] A. Triolo, O. Russina, B. Fazio, G. Battista Appetecchi, M. Carewska, S. Passerini, J. Chem. Phys. 130 (2009) 164521.
[16] Z.B. Zhou, H. Matsumoto, K. Tatsumi, Chem. Eur. J. 12 (2006) 2196.
[17] I. Mukhopadhyay, C.L. Aravinda, D. Borissov, W. Freyland, Electrochim. Acta 50 (2005) 1275.
[18] P. Hapiot, C. Lagrost, Chem. Rev. 108 (2008) 2238.

[19] H. Ohno, in: F. Endres, A.P. Abbott, D.R. MacFarlane (Eds.), Electrodeposition from Ionic Liquids, Wiley-VCH Verlag GmbH & Co., 2008 (Chapter 3).
[20] S. Zein El Abedin, N. Boressinko, F. Endres, Electrochem. Commun. 6 (2004) 510.
[21] J. Salminen, N. Papaiconomou, R.A. Kumar, J.M. Lee, J. Kerr, J. Newman, J.M. Prausnitz, Fluid Phase Equilib. 261 (2007) 421.
[22] D.D. Shivagan, P.J. Dale, A.P. Samantilleke, L.M. Peter, Thin Solid Films 515 (2007) 5899.
[23] Y. Castrillejo, M.R. Bermejo, A.M. Martinez, C. Abejon, J. Appl. Electrochem. 29 (1999) 65.
[24] M. Mohamedi, S. Martinet, J. Bouteillon, J.C. Poignet, Electrochim. Acta 44 (1998) 797.
[25] M.-H. Yang, M.-C. Yang, I.-W. Sun, J. Electrochem. Soc. 150 (2003) C544.
[26] J.S.-Y. Liu, I.W. Sun, J. Electrochem. Soc. 144 (1997) 140.
[27] R.E. Visco, J. Electrochem. Soc. 112 (1965) 932.
[28] M. Mohamedi, J. Bouteillon, J.C. Poignet, Electrochim. Acta 41 (1996) 1495.
[29] Y.-C. Fu, Y.-Z. Su, H.-M. Zhang, J.-W. Yan, Z.-X. Xie, B.-W. Mao, Electrochim. Acta 55 (2010) 8105.
[30] M.K. Carpenter, M.W. Verbrugge, J. Mater. Res. 9 (1994) 2584.